Optical Detection of Single-Electron Spin Resonance in a Quantum Dot

Martin Kroner,[1] Kathrina M. Weiss,[1] Benjamin Biedermann,[1] Stefan Seidl,[1] Stephan Manus,[1] Alexander W. Holleitner,[1] Antonio Badolato,[2] Pierre M. Petroff,[2] Brian D. Gerardot,[3] Richard J. Warburton,[3] and Khaled Karrai[1]

[1]*Center for NanoScience and Fakultät für Physik, Ludwig-Maximilians-Universität, 80539 München, Germany*
[2]*Materials Department, University of California, Santa Barbara, California 93106, USA*
[3]*School of Engineering and Physical Sciences, Heriot-Watt University, Edinburgh EH14 4AS, United Kingdom*

(Received 25 October 2007; published 16 April 2008)

We demonstrate optically detected spin resonance of a single electron confined to a self-assembled quantum dot. The dot is rendered dark by resonant optical pumping of the spin with a laser. Contrast is restored by applying a radio frequency (rf) magnetic field at the spin resonance. The scheme is sensitive even to rf fields of just a few μT. In one case, the spin resonance behaves as a driven 3-level λ system with weak damping; in another one, the dot exhibits remarkably strong (67% signal recovery) and narrow (0.34 MHz) spin resonances with fluctuating resonant positions, evidence of unusual dynamic processes.

DOI: 10.1103/PhysRevLett.100.156803 PACS numbers: 73.21.La, 78.67.Hc

The control of few-level systems is a major challenge for the development of novel computation schemes based on quantum states. Solid state-based nanostructures can be tailored and tuned *in situ*, offering significant advantages over conventional quantum systems such as atoms and ions. Furthermore, in a strongly quantized solid state system, electron spin is remarkably robust as the quantization suppresses phonon-related spin relaxation [1–3], adding weight to proposals using spin as a qubit [4]. Recently, spin relaxation times as long as $T_1 \sim 1$ s [2,5] and a lower bound on the coherence time T_2 of 1 μs [6–8] have been established on quantum dots. It is clearly of fundamental importance to develop spin resonance schemes with single spin resolution. In the longer term, spin resonance provides the capability of performing arbitrary spin rotations in the Bloch sphere; in the shorter term, it provides unique insights into the complex spin interactions in the solid state environment. Single spin resonance has been achieved on an electrostatically defined quantum dot with electrical detection [9]. An alternative is to detect the spin resonance optically. This is potentially very sensitive because of the in-built amplification of $\sim 10^5$–10^7 since absorption of a microwave photon leads to absorption of an optical photon. While optically detected single-electron spin resonance on the nitrogen-vacancy center, a deep impurity level in diamond, is established [10], optically detected single-electron spin resonance on a quantum dot has not been demonstrated before.

Our electron spin resonance (ESR) scheme is shown in Fig. 1(a). A single electron is confined to the dot and a magnetic field is applied, splitting the electron spin states, $|\downarrow\rangle$ and $|\uparrow\rangle$, by the Zeeman energy. The first step is to project the electron into, say, the $|\downarrow\rangle$ state. We do this with optical pumping: a laser drives the $|\uparrow\rangle \leftrightarrow |\uparrow\downarrow, \Uparrow\rangle$ transition where $|\uparrow\downarrow, \Uparrow\rangle$ represents the X^{1-} exciton consisting of two spin-paired electrons and a spin-up hole. Spontaneous emission in the presence of some symmetry breaking projects the electron into the $|\downarrow\rangle$ state where the population is shelved. The signature for spin initialization is the disappearance of a signal related to resonant Rayleigh scattering of the optical laser [11–13]. The second step is to apply a radio frequency (rf) magnetic field at the Zeeman frequency. The rf field drives the spin resonance transition, $|\downarrow\rangle \leftrightarrow |\uparrow\rangle$. This causes the $|\uparrow\rangle$ state to be repopulated, reestablishing the Rayleigh scattering. The scheme is a contemporary application of magnetic resonance developed originally with Hg atoms, replacing a huge ensemble of atoms with a single

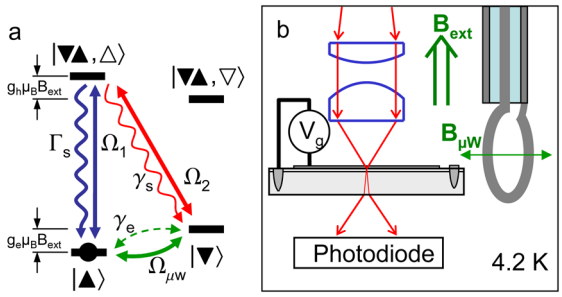

FIG. 1 (color online). (a) Level scheme for optically detected spin resonance. The electron spin states, $|\uparrow\rangle$ and $|\downarrow\rangle$, are split by the electron Zeeman energy $g_e\mu_B B_{\text{ext}}(g_e < 0)$. $|\uparrow\downarrow, \Uparrow\rangle$ denotes the spin-up exciton state, X^{1-}. The σ^+-polarized transition $|\uparrow\rangle \leftrightarrow |\uparrow\downarrow, \Uparrow\rangle$ is driven on resonance with a coherent laser. The spin resonance transition, $|\downarrow\rangle \leftrightarrow |\uparrow\rangle$, is driven with an oscillating magnetic field $B_{\mu\text{W}}$ at right angles to the dc external magnetic field, B_{ext}. Incoherent processes are spontaneous radiative decay, $|\uparrow\downarrow, \Uparrow\rangle \rightarrow |\uparrow\rangle$ (fast), $|\uparrow\downarrow, \Uparrow\rangle \rightarrow |\downarrow\rangle$ (slow); and spin relaxation, $|\downarrow\rangle \leftrightarrow |\uparrow\rangle$ (very slow). (b) Schematic of experimental setup. The laser excitation at wavelengths around 950 nm is focused onto the sample with an objective with numerical aperture 0.5 and gives a spot size of ~ 1 μm at the sample. The transmitted light is detected with an *in situ* photodiode. A dc magnetic field, B_{ext}, is applied perpendicular to the sample. An ac magnetic field, $B_{\mu\text{W}}$, is generated with a closed loop antenna of diameter 2 mm positioned 2 mm along its axis from the quantum dot. The loop is connected to a microwave oscillator via a high frequency cable. The objective, sample, and antenna are all at 4.2 K.

quantum dot, an incoherent source with a laser, and fluorescence detection with Rayleigh scattering.

We perform spin resonance on single InAs/GaAs self-assembled quantum dots. The dots are embedded in a field effect structure that allows for controlled charging with single electrons [14,15]. In the present device, the tunneling barrier is 25 nm thick and the back contact is a two-dimensional electron gas with carrier concentration 10^{12} cm^{-2}. The sample is mounted in a 4 K optical microscope, a magnetic field of $B_{\text{ext}} = 0.5$ T is applied in the growth direction (Faraday geometry), and a voltage V_G is applied to a surface Schottky barrier in order to trap a single electron in a particular dot, Fig. 1(b). The interaction with a narrow band laser tuned to the fundamental cross-gap transition is detected in transmission: a dip with linewidth ~ 2 μeV is observed on resonance [16]. The quantum dot is tuned relative to the laser by sweeping V_G, which shifts the exciton through the quantum confined Stark effect. The microwave field is generated by a single loop antenna [Fig. 1(b)] with a geometry designed to emit over a broad frequency spectrum. The investigated quantum dot lies close to the antenna on its symmetry axis ensuring that the dot experiences only the near field of the antenna, which contains a magnetic but nearly no electric field component. From the geometry and the electrical characteristics of the setup, we estimate the ac magnetic field $B_{\mu W}$ to be a few μT.

The primary signature of optical spin pumping is a loss of transmission signal as a magnetic field is applied [11–13], Fig. 2. The hyperfine interaction plays a dual role here [13]. In the absence of any induced nuclear polarization, the electron experiences an Overhauser field B_N on account of the incomplete cancellation of the magnetic fields generated by each nucleus in the quantum dot. First, for small B_{ext}, fluctuations in B_N induce rapid electron spin relaxation [13,17]. As B_{ext} increases, this relaxation mechanism is suppressed on account of the energetic mismatch in nuclear and electronic Zeeman energies. Second, the in-plane component of B_N is responsible for the symmetry breaking required for the "forbidden" $|\uparrow\downarrow, \Uparrow\rangle \rightarrow |\downarrow\rangle$ transition, Fig. 1(a), tilting the electron (but not the exciton) quantization axis away from the z axis. The in-plane Overhauser field is ~ 30 mT for these dots, as deduced either from the dot size and hyperfine coupling constants or from an interpretation of optical spin pumping [13]. The spin admixture is small at $B_{\text{ext}} = 0.5$ T but nevertheless sufficient for spin pumping. The spin relaxation rate can also be controlled via V_G: at the edges of the Coulomb blockade plateau, spin relaxation is rapid via a spin swap with the back contact, a cotunneling process [11–13,18], but highly suppressed in the plateau center.

One of the challenges in the ESR experiment is that the electron g factor, g_e, for a given quantum dot is unknown. g_e varies in our case from -0.5 to -0.8 from dot to dot. Furthermore, in the Faraday configuration, conventional laser spectroscopy measures only the sum of the electron and hole Zeeman energies, and the hole Zeeman energy is typically 2 or 3 times larger than the electron Zeeman energy. Compounding this, the ESR is potentially very narrow in frequency space. This represents a spectral "needle in a haystack" problem. To solve it, we have developed a laser spectroscopy technique to determine g_e. The concept is to exploit the sensitivity of the spin pumping to any transition, even a very weak one, involving

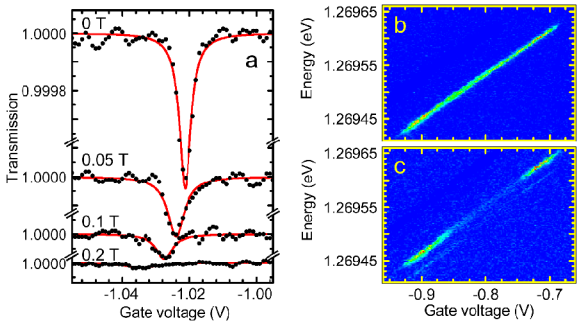

FIG. 2 (color online). Spin shelving via optical pumping. (a) Differential transmission data on a single quantum dot at 4.2 K as a function of the applied magnetic field, B_{ext}, recorded with a V_G at the center of the charging plateau. The contrast disappears as B_{ext} increases. (b),(c) Color scale plots of the V_G dependence. (b) At $B_{\text{ext}} = 0$, the optical signal is maintained across the plateau; (c) at $B_{\text{ext}} = 0.5$ T, the optical signal is suppressed in the plateau center signifying spin shelving, but recovers at the plateau edges signifying rapid spin relaxation via cotunneling. In (c), the two resonances correspond to the two Zeeman-split exciton transitions. The polarization is right-handed circularly polarized with a weak left-handed component.

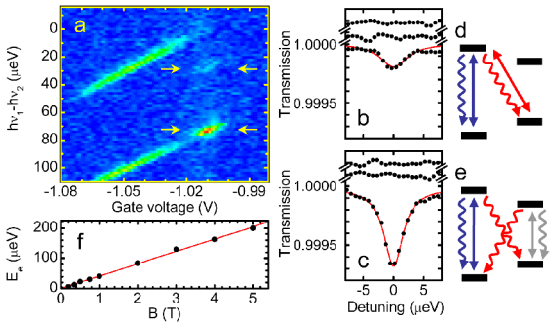

FIG. 3 (color online). Optical characterization with 2 coherent lasers. The energy of laser 1 is chosen to come into resonance with the higher energy Zeeman transition, $|\uparrow\rangle \leftrightarrow |\uparrow\downarrow, \Uparrow\rangle$, at $V_G = -1.01$ V where the transmission contrast is immeasurably small owing to spin shelving in the $|\downarrow\rangle$ state. The power of laser 1 is 1 nW. The energy of a second laser, $h\nu_2$, with power 1 nW is redshifted relative to laser 1, and the differential transmission is recorded as a function of V_G. Both lasers are linearly polarized. The process is repeated for different $h\nu_2$. (a) The data as a color plot. (b),(c) The transmission spectra for laser 1 alone, for laser 2 alone, and for laser 1 and laser 2 (offset for clarity) for the two double resonances marked in (a). (d),(e) The respective interpretations of the double resonances in terms of the level diagram, Fig. 1. (f) Difference in absorbed photon energy of the two lasers, as in (d), against magnetic field with a linear fit.

the shelved electron spin state. As shown in Fig. 3(d), we apply two laser fields, the first on resonance with the strong $|\uparrow\rangle \leftrightarrow |\uparrow\downarrow, \Uparrow\rangle$ transition, which projects the spin into the $|\downarrow\rangle$ state, and the second tuned in energy to the weak $|\downarrow\rangle \leftrightarrow |\uparrow\downarrow, \Uparrow\rangle$ transition. On resonance, the second laser frustrates the spin shelving induced by the first laser, leading to a recovery of the optical transmission signal.

To implement this scheme for determining g_e, we choose the frequency of the first laser ν_1 such that it comes into resonance with the higher energy Zeeman transition, $|\uparrow\rangle \leftrightarrow |\uparrow\downarrow, \Uparrow\rangle$ at a V_G far from the plateau edge (-1.01 V in Fig. 3), and the transmission signal is therefore quenched by efficient spin pumping. The frequency of the second laser, ν_2, is then gradually redshifted relative to the first. Both lasers are linearly polarized so that all circularly polarized transitions can be pumped and both lasers are incident on the same transmission detector. For each ν_2 we scan the gate voltage, Fig. 3(a). The two regions of high transmission contrast between -1.06 and -1.03 V represent the interaction of the second laser with the two Zeeman-split transitions, $|\uparrow\rangle \leftrightarrow |\uparrow\downarrow, \Uparrow\rangle$ and $|\downarrow\rangle \leftrightarrow |\uparrow\downarrow, \Downarrow\rangle$, at the plateau edge where the contrast is large. For $V_G > -1.03$ V, spin shelving starts and the contrast from the strong Zeeman transitions quenches. However, there are two values of $h\nu_2$ where contrast is reestablished at $V_G = -1.01$ V signifying double resonances, shown by arrows in Fig. 3(a). Figures 3(b) and 3(c) show line cuts through the two double resonances. The spectra were measured with each laser separately (no visible transmission dip) and then with both together (transmission dip) and are interpreted with the level diagrams of Figs. 3(d) and 3(e). In 3(c) and 3(e), laser 1 pumps the higher energy Zeeman transition, and laser 2 pumps the lower energy Zeeman transition. Laser 2 frustrates the spin shelving from laser 1 and vice versa, leading to a recovery in contrast, a repumping phenomenon [11]. In 3(b) and 3(d), however, laser 2 pumps the weaker cross-transition, and $h\nu_1 - h\nu_2$ corresponds to the electron Zeeman energy, allowing its experimental determination. $h\nu_1 - h\nu_2$ depends linearly on B_{ext}, passing through the origin, exactly the behavior for a Zeeman splitting, Fig. 3(f), yielding $g_e = -0.56 \pm 0.05$ for this particular dot.

The power of our scheme for determining g_e is that, by monitoring the strong $|\uparrow\rangle \leftrightarrow |\uparrow\downarrow, \Uparrow\rangle$ transition in the spin pumping regime, we can detect the presence of the weak $|\downarrow\rangle \leftrightarrow |\uparrow\downarrow, \Uparrow\rangle$ transition, which is completely hidden either in conventional laser spectroscopy or photoluminescence characterization. The detection of ESR proceeds in a similar way, in this case the spin resonance frustrates the spin shelving.

We concentrate on two dots, dot A with $g_e = -0.56 \pm 0.05$ and dot B with $g_e = -0.63 \pm 0.05$. At $B_{\text{ext}} = 0.5$ T, the predicted ESR frequency is 3.9 ± 0.3 GHz (4.4 ± 0.3 GHz) for dot A (B). To search for ESR, we scanned the rf over a 1 GHz bandwidth with a resolution of 0.1 MHz integrating over 1 s. To ensure that the optical laser remains in resonance throughout, we operated in a regime of V_G close to the plateau edges where cotunneling is sufficiently strong to give us a small optical signal. For each rf, we performed a V_G sweep. Figure 4(a) is a contour plot of V_G (optical detuning) versus rf for dot A; Fig. 4(g) optical signal versus rf at zero optical detuning for dot B. For all rf, the optical resonance can be just made out in Fig. 4, demonstrating that the optical resonance is maintained throughout. However, at very specific microwave frequencies, there is an increase in optical signal. For dot A, the signal recovers to 67% of its value at $B_{\text{ext}} = 0$ and the ESR linewidth is extremely small, 0.34 MHz. For dot B, the signal recovery is smaller, 12%, and the ESR linewidth is larger, 24 MHz. These resonances correspond to ESR because, first, for both dots the resonances occur at the known Zeeman frequencies, and second, no resonances were ever observed, with the rf source turned off.

For dot B, each ESR experiment yields the same resonance position, contrast, and linewidth. This shows that for dot B the integration time permits ensemble averaging. We therefore analyze dot B using the steady state solution to the density matrix with Markovian decay dynamics, treating both optical and rf couplings nonperturbatively. The assumption is that over the course of the integration, the z component of B_N averages to zero, and that the in-plane component can be taken as the root-mean-square (rms) value, $B_{N,xy}$. We consider 3 levels, $|\uparrow\rangle$, $|\downarrow\rangle$, and $|\uparrow\downarrow, \Uparrow\rangle$ with a coherent optical coupling between $|\uparrow\rangle$ and $|\uparrow\downarrow, \Uparrow\rangle$

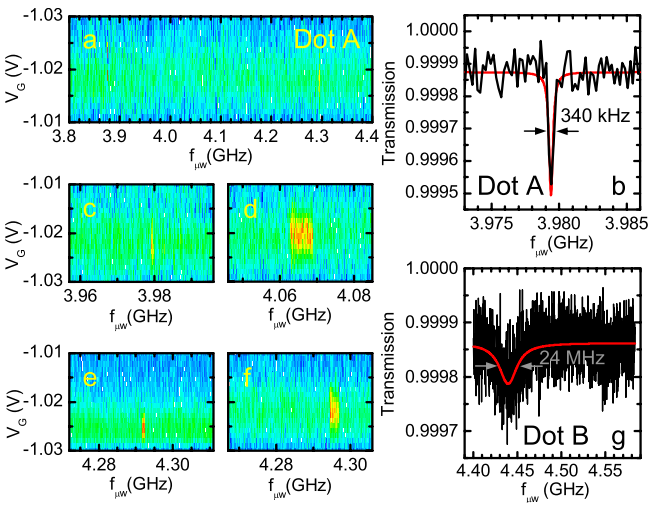

FIG. 4 (color online). Optically detected spin resonance for dot A at $B_{\text{ext}} = 0.5$ T. Color scale plot of the optical transmission signal with microwave frequency, $f_{\mu\text{W}}$, along the x axis, and gate voltage (equivalently optical detuning, δ) along the y axis. The Stark shift $d\delta/dV_G$ is 0.9 μeV/mV. For each microwave frequency, the gate voltage is swept from -1.01 to -1.03 V. The strong signal close to 4.3 GHz is the electron spin resonance (ESR). (c)–(f) Other experimental runs on the same dot under identical conditions; (b) optical transmission versus microwave frequency at zero optical detuning from (c) showing ESR close to 3.98 GHz. (g) Optically detected spin resonance for dot B at 0.5 T and zero optical detuning. The black line corresponds to the experimental data; the red line to the theory.

with Rabi energy $\hbar\Omega_1$ and a coherent rf coupling between $|\uparrow\rangle$ and $|\downarrow\rangle$ (ESR) with Rabi energy $\hbar\Omega_{\mu W} = g_e\mu_B B_{\mu W}$ where μ_B is the Bohr magneton. The master equation includes decay terms: spontaneous radiative recombination from $|\uparrow\downarrow, \Uparrow\rangle$ to $|\uparrow\rangle$ at rate Γ_s; spontaneous radiative recombination from $|\uparrow\downarrow, \Uparrow\rangle$ to $|\downarrow\rangle$ at rate $\gamma_s (\gamma_s \ll \Gamma_s)$; and spin relaxation $|\uparrow\rangle \leftrightarrow |\downarrow\rangle$ at rate γ_e. The transmission signal depends on the optical susceptibility. Γ_s is known from the measured radiative decay rates on these dots and $\hbar\Omega_1$ is known from saturation curves of the optical resonance without spin pumping. The branching ratio γ_s/Γ_s depends on $B_{N,xy}$. For $B_{N,xy} \ll B_{\text{ext}}$, $\gamma_s/\Gamma_s = (B_{N,xy}/2B_{\text{ext}})^2 = 0.08\%$ with $B_{N,xy} = 28$ mT [13]. To fit the ESR, Fig. 4(g), we require $\hbar\gamma_e = 2.4$ peV ($T_1 = 0.27$ ms, limited by cotunneling) and $\hbar\Omega_{\mu W} = 0.36$ neV corresponding to $B_{\mu W} = 11$ μT for $g_e = -0.63$. This $B_{\mu W}$ agrees reasonably with the rough estimate based on Fig. 1. Figure 4(g) shows that we achieve an excellent fit to the ESR data. The theory shows that in general the ESR linewidth depends on both the optical and microwave couplings. In Fig. 4(g), the optical coupling makes the larger contribution. However, if $B_{\mu W}$ is increased by an order of magnitude, the theory predicts that the ESR signal on resonance will increase from 12% to close to 100% with an increase in the linewidth through power broadening of the ESR. Accessing this regime is clearly possible with a microscopic rather than a macroscopic antenna [9].

Dot A behaves differently from dot B: from run to run, the ESR frequency fluctuates by ± 150 MHz, Fig. 4, translating into a variation in magnetic field of ± 19 mT. The obvious culprit is the nuclear field: the fluctuations in resonance position correspond to the rms average of $B_{N,z}$ [13]. In dot A therefore, fluctuations in $B_{N,z}$ are slow relative to the measurement, unlike dot B. In fact, for dot A where a V_G sweep was performed for each microwave frequency, Fig. 4 shows that $B_{N,z}$ must remain constant for tens of seconds. Remarkably, despite the difference in the nuclear field correlation time t_N ($t_N \gg 1$ s for dot A; $t_N \ll 1$ s for dot B), the optical properties of dots A and B are the same. The origin of the different t_N lies either in the differing strain fields in the two dots—strain influences the quadrupole interaction of each nucleus leading to position-dependent and nonequidistant nuclear Zeeman splittings [19]—or in differences in the electron tunneling dynamics. t_N for dot A is reminiscent of bulk GaAs [20]; t_N for dot B is consistent with the decay time of dynamic nuclear spin polarization in an InGaAs dot where, in the presence of an electron, decay times of $\sim$ ms were determined [21].

The large ESR signals and narrow ESR linewidths are very striking for dot A, Fig. 4. It is impossible to reproduce the signal and linewidth with the 3-level model without reducing the optical power by an unrealistic factor of $\sim$100. In some cases, Figs. 4(d)–4(f), the ESR has a strange line shape, with hints that the ESR locks on to the rf driving field over a band of frequencies. There is, therefore, a backaction of the nuclear spins on the electron spin; equivalently, the ESR cannot be described with a constant $B_{N,xy}$. We speculate that the cycle in the ESR detection, $|\downarrow\rangle \rightarrow |\uparrow\rangle \rightarrow |\uparrow\downarrow, \Uparrow\rangle \rightarrow |\downarrow\rangle$, leads to some alignment of the nuclear field when t_N is large. A significant nuclear polarization is very difficult to achieve with resonant excitation [22,23] and, in fact, can be ruled out as a large nuclear polarization would detune the dot from the laser. Instead, it is possible that our experiment aligns the residual field, B_N: when B_{ext}, $B_{N,z}$, and microwave frequency satisfy the ESR condition, B_N and the electron spin become aligned, at which point $B_{N,xy} \rightarrow 0$, electron spin shelving becomes very slow, and the full optical signal is recovered. In this picture, the ESR resonance fluctuates in frequency as the exact position depends on $B_{N,z}$, which is both random and long-lived for dot A. A theory treating the full electron *and* nuclear spin dynamics on an equal footing is required [24].

Financial support from the DFG (SFB 631 and Excellence Cluster NIM) and EPSRC (U.K.) is gratefully acknowledged. We thank Jörg Kotthaus and Patrick Öhberg for helpful discussions.

[1] V. N. Golovach, A. Khaetskii, and D. Loss, Phys. Rev. Lett. **93**, 016601 (2004).
[2] M. Kroutvar *et al.*, Nature (London) **432**, 81 (2004).
[3] J. M. Elzerman *et al.*, Nature (London) **430**, 431 (2004).
[4] D. Loss and D. P. DiVincenzo, Phys. Rev. A **57**, 120 (1998).
[5] S. Amasha *et al.*, Phys. Rev. Lett. **100**, 046803 (2008).
[6] J. R. Petta *et al.*, Science **309**, 2180 (2005).
[7] A. Greilich *et al.*, Science **313**, 341 (2006).
[8] M. H. Mikkelsen *et al.*, Nature Phys. **3**, 770 (2007).
[9] F. H. L. Koppens *et al.*, Nature (London) **442**, 766 (2006).
[10] F. Jelezko *et al.*, Phys. Rev. Lett. **92**, 076401 (2004).
[11] M. Atatüre *et al.*, Science **312**, 551 (2006).
[12] M. Kroner *et al.*, Int. J. Mod. Phys. B **21**, 1307 (2007).
[13] J. Dreiser *et al.*, Phys. Rev. B **77**, 075317 (2008).
[14] R. J. Warburton *et al.*, Nature (London) **405**, 926 (2000).
[15] S. Seidl *et al.*, Phys. Rev. B **72**, 195339 (2005).
[16] A. Högele *et al.*, Phys. Rev. Lett. **93**, 217401 (2004).
[17] I. A. Merkulov, A. L. Efros, and M. Rosen, Phys. Rev. B **65**, 205309 (2002).
[18] J. M. Smith *et al.*, Phys. Rev. Lett. **94**, 197402 (2005).
[19] R. I. Dzhioev and V. L. Korenev, Phys. Rev. Lett. **99**, 037401 (2007).
[20] D. Paget, Phys. Rev. B **25**, 4444 (1982).
[21] P. Maletinsky, A. Badolato, and A. Imamoglu, Phys. Rev. Lett. **99**, 056804 (2007).
[22] A. Imamoglu *et al.*, Phys. Rev. Lett. **91**, 017402 (2003).
[23] H. Christ, J. I. Cirac, and G. Giedke, Phys. Rev. B **75**, 155324 (2007).
[24] J. Danon and Y. V. Nazarov, Phys. Rev. Lett. **100**, 056603 (2008).